Journal of ELECTRONIC MATERIALS, Vol. 48, No. 7, 2019
https://doi.org/10.1007/s11664-019-07206-6

Electronic and Bandgap Tuning of Hydrogenated Ti-doped CdO Semiconductor

A.A. DAKHEL[1,3] and H. HAMAD[2]

1.—Department of Physics, College of Science, University of Bahrain, P.O. Box 32038, Zallaq, Kingdom of Bahrain. 2.—University of Abu Dhabi, P.O. Box 59911, Abu Dhabi, United Arab Emirates. 3.—e-mail: adakhil@uob.edu.bh

The physical vapour deposition method was employed to study and improve the optoelectronic properties of CdO as a transparent conducting oxide (TCO), using the doping technique. Different small amounts of titanium ions were incorporated into CdO thin films deposited on glass substrates and were used to study the conduction parameters CPs (conductivity/resistivity, carrier mobility, and carrier concentration) together with the optical transparency. Different diagnostic methods, x-ray diffraction, optical absorption spectroscopy, scanning electron microscopy and electrical measurements were used to study and characterize the deposited thin films. The results of this work, revealed that the ultimate TCO CPs were obtained with Ti doping level of 0.3–0.6 wt.%; the mobility$\sim$ 40 cm^2/V.s, carrier concentration $\sim 7\times1020$ cm^{-3} and conductivity $\sim 2.88 \times 10^3$ S/cm. The results, also revealed that Ti doping strongly enhanced the [111] preferred orientation growth of CdO films especially with 0.3 wt.%.

Key words: Cadmium-titanium oxide, Ti-doped CdO, TCO

INTRODUCTION

Cadmium oxide thin films have a unique combination of high electrical conductivity and optical transparency especially in the NIR spectral region. From that point of view, it is belonged to the group of transparent conducting oxides (TCO) like In_2O_3, Ga_2O_3, SnO_2, and ZnO, which have numerous optoelectronic applications of the solar-cell field and manufacturing of smart windows, etc.[1–3] The reasons for the optical and electrical properties of any TCO are their natural non-stoichiometric point defects like oxygen vacancies (V_O) and metal interstitials (M_i). Therefore, the development in their TCO properties for the highest performance should base on the control of those internal natural point defects. It was found that the optoelectronic properties could be controlled and developed by doping/incorporation with different types of impurity ions.[4–7] CdO has rock-salt cubic (Fm^{-3} m) structure with a lattice parameter of 0.4695 nm.[8] It has a *n*-type degenerate semiconducting properties with resistivity (10^{-2}–10^{-4} Ω cm). The optical properties of CdO films show translucency in the Vis spectral region and good transparency in the NIR spectral region with the optical bandgap in the range of ~2.2–2.7 eV depending on the preparation conditions.[1,2]

In the present work, films of CdO incorporated by different amounts of Ti ions were prepared and their optoelectronic properties were studied. Titanium ions of radius 0.06 nm (VI coordination) are considerably smaller than Cd ions (0.095 nm).[9] Therefore, Ti ions were supposed to be able to substitute for Cd^{2+} ions in CdO lattice forming substitutional solid solution (SSS) without introducing a significant distortion in the cubic structure of CdO lattice unit cell (UC) only for small concentrations. Thus, small Ti concentrations of less that $\sim$ 1 wt.% were chosen in the present work. Additionally, it was supposed that annealing in H_2 atmosphere should have effect on the physical properties including (1) to improve the distribution

(Received November 14, 2018; accepted April 6, 2019; published online April 16, 2019)

by tossing of the dopant Ti ions throughout the CdO sample films and (2) to create oxygen vacancies (V_O) in order to improve the TCO properties. Creation V_O needs to assist dopant Ti ions, which can play role of a catalyst in dissociation of H_2 molecules.[10]

Generally, incorporation of Ti ions in CdO lattice is expected to improve its electronic transport properties. The effect of Ti doping on the physical properties of some TCO films was previously studied, like ZnO,[11,12] In_2O_3,[13] and SnO_2.[14] Previous Ti-incorporated CdO (CdO:Ti) samples were prepared by physical vapor deposition (sputtering and laser) of a mixture of CdO/TiO2 powders by many researchers.[15–18]

EXPERIMENTAL DETAILS

CdO thin films doped with different amounts of titanium ions and annealed in hydrogen atmosphere (CdO:Ti-H) were deposited on cleaned soda-lime glass substrates (from Sigma-Aldrich). At start, the CdO materials and Ti (from Aldrich Chemicals) were thermally evaporated in vacuum environment by alumina baskets (Midwest tungsten service, USA) to avoid the inclusion of unwanted impurities in the films. A piezoelectric Microbalance sensor (Philips FTM5) fixed close to the substrates was used to monitor and controlled the evaporated masses. The deposited thin films/glass substrates were annealed in the air atmosphere at 400°C for about1 h followed by keeping them cool down inside the oven to room temperature. Then, followed by annealing these samples in static H_2 atmosphere at 350°C for 15 min. Using a MP100-M spectrometer (Mission Peak Optics Inc., USA), film thicknesses were measured after annealing and they were in the range of 0.12–0.26 μm. Five different samples of the prepared Ti-doped CdO film were chosen. Each sample contained Ti dopant of a certain amount,

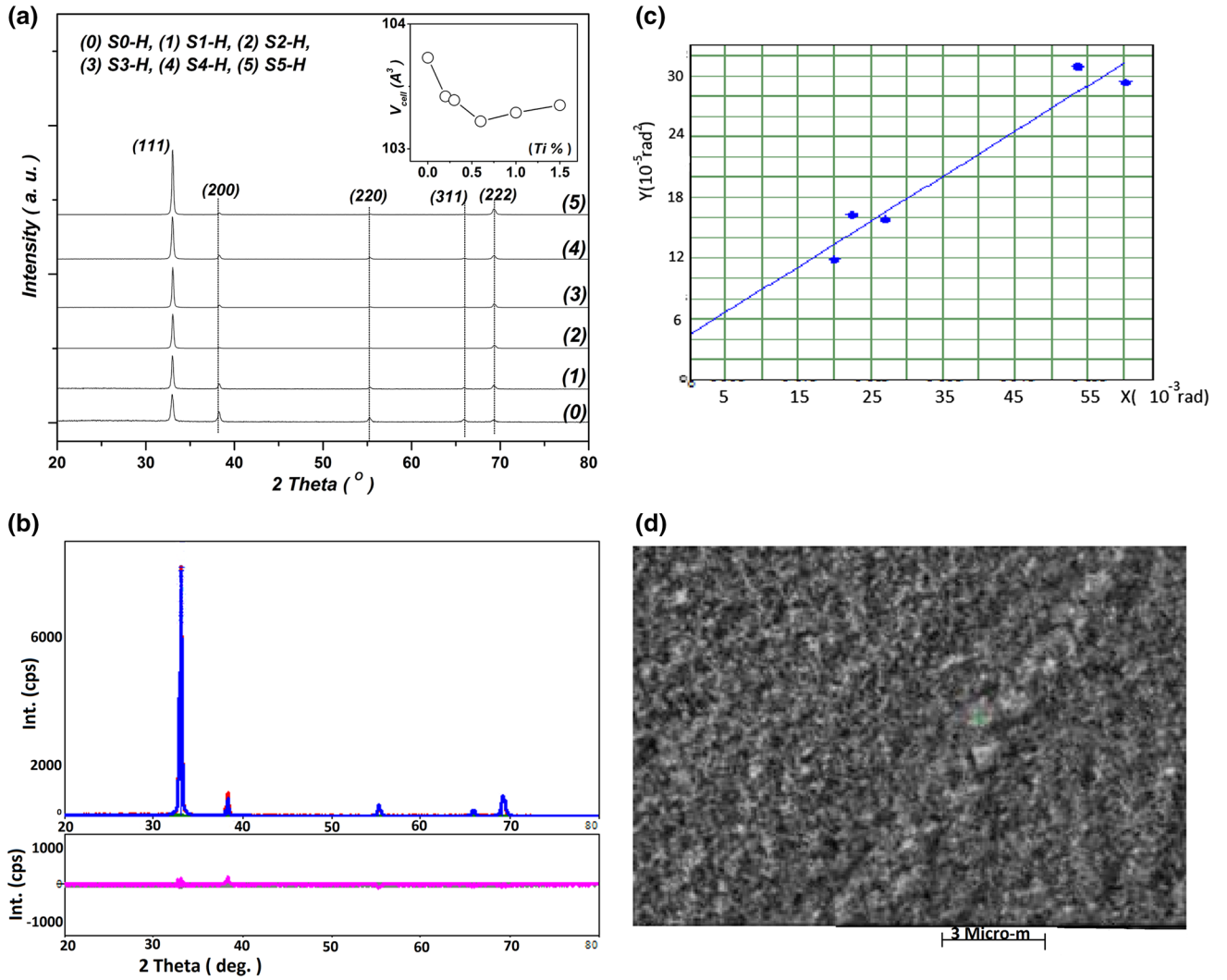

Fig. 1. XRD patterns of hydrogenated undoped and Ti-doped CdO films and the inset shows the variation of cell volume with Ti doping level (a), Rietveld refinements of S4-H film: experimental data; solid pink line (down): intensity difference, calculated pattern; red solid line (b), Williamson-Hall plot for S4-H sample (c), and SEM micrographs for S4-H sample(d).

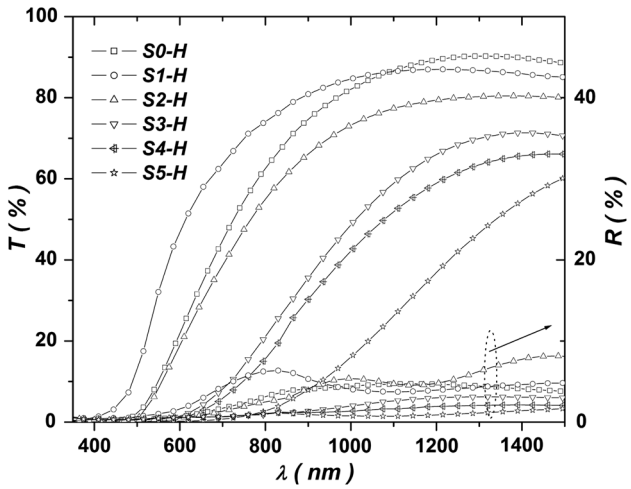

Fig. 2. Spectral transmittance, $T(\lambda)$ and reflectance, $R(\lambda)$ of hydrogenated undoped and Ti-doped CdO films.

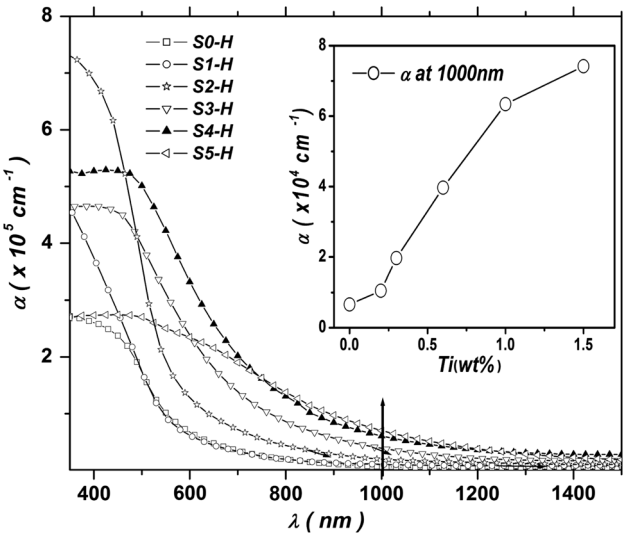

Fig. 3. Spectral calculated absorption coefficient, $\alpha(\lambda)$ of hydrogenated undoped and Ti-doped CdO films. The inset shows the variation of absorption coefficient α at 1000 nm with Ti% doping level.

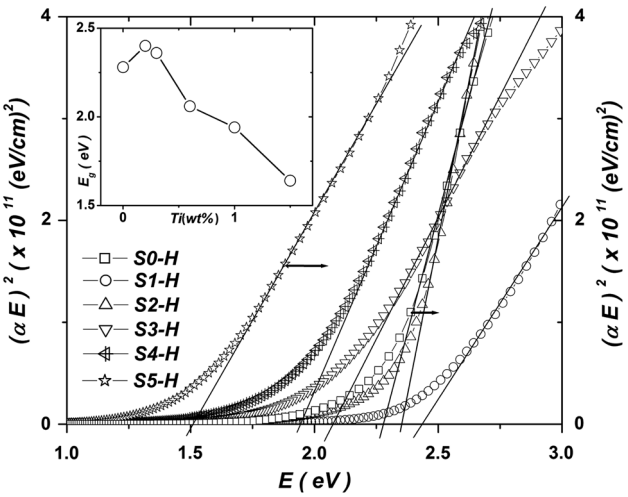

Fig. 4. Tauc plot for all for hydrogenated undoped and Ti-doped CdO films. The inset shows the variation of band gap Eg with Ti% doping level.

which was estimated by a scanning electron microscope, SEM (SEM/EDX microscope Zeiss EVO) to be ~ 0.2 wt.%, 0.3 wt.%, 0.6 wt.%, 1 wt.%, 1.5 wt.% (each film sample was referred as S1-H, S2-H, S3-H, S4-H, and S5-H, respectively) in addition to the reference of the un-doped CdO film (S0-H sample). The crystal structures of thin films were examined by x-ray diffraction technique (XRD), using a Rigaku Ultima-VI x-ray with Cu-K_α line. The structural analyses, including lattice parameters and crystallite size (CS) were carried out respectively by Rietveld refinement and Williamson-Hall method, which are in the content of the built-in PDXL software programs of the used XRD apparatus. Shimadzu UV-3600 double beam spectrophotometer was used to measure the optical normal transmittance T(λ) and reflectance R(λ) of each film sample within the spectral range (300–1500) nm. The electrical measurements were carried out with a standard Van-der-Pauw technique using silver paste dot contacts in a magnetic field of about 1 T and using a Keithley 195A digital multimeter and a Keithley 225 current source.

STRUCTURE ANALYSIS

The XRD patterns of undoped CdO-H and CdO:Ti-H films deposited on glass substrates are shown in Fig. 1a. The normalised reflections of the XRD patterns were indexed according to the known standard cubic structure (Fm-3 m).[8] The patterns reveal that the energetically preferred [111] orientation of pristine CdO films was enhanced with Ti-ions doping. The variation in the degree of [111] preferred-orientation growth of the investigated films by inclusion of Ti ions confirmed the doping/incorporation process of Ti ions in CdO lattice. The texture coefficient; $TC_{[111]} = [nI_{[111]}/I_{0[111]}]/[\sum' I(h'k'l')/I_0(h'k'l')]$,[19] can be used to study the growth degree of the preferential orientation in [111] direction, where $I_{[hkl]}$ and $I_{0[hkl]}$ are the integrated intensities of certain [h*k*l] reflection from the film sample and the standard polycrystalline powder, which is listed in Ref. 8. The sum in the equation runs over the total number (n = 4) of the recorded reflections. The highest $TC_{[111]}$ value was (3.9/4) for S2-H (0.3 wt.%) sample, which shows about total [111] orientation as shown in (Fig. 6). Such enhancement of [111] orientation of host CdO film was also observed for other metallic dopants, such as Fe, Cr, Ce.[5,20,21] Therefore, considering $TC_{[111]}$ as a gauge of film crystallinity, then it must have a great control on the electronic scattering at crystallite and grain boundaries (CB and GB) or on

the carrier mobility (μ). Subsequently, there must be a relation between μ and TC, and as a result one can predict that the maximum mobility (μ) should be observed with S2-H sample (Fig. 6).

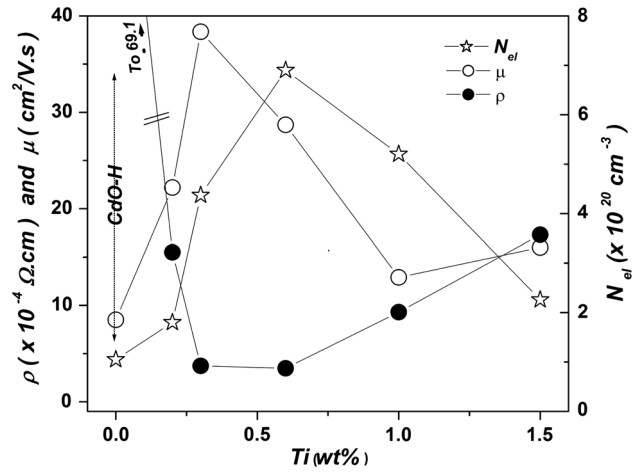

Fig. 5. Conduction parameters (CPs) variations with Ti doping level in the film samples.

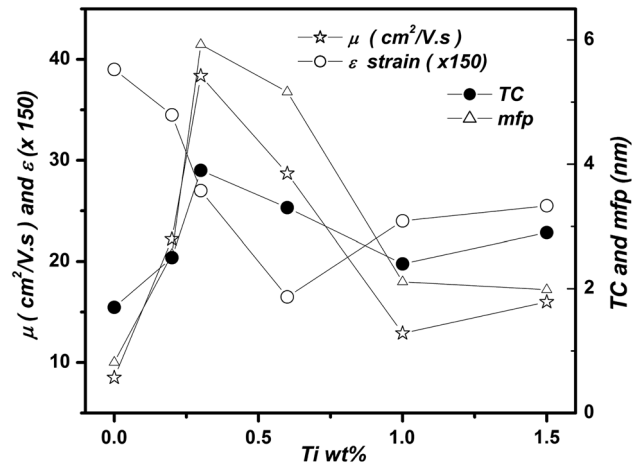

Fig. 6. Dependence of structural parameters (TC and ε) and CPs (mobility, μ and mean free path, mfp) with incorporation level of CdO films.

Moreover, Fig. 1a reveals that doping with Ti and hydrogenation did not modify the ordinary cubic crystalline structure of CdO. Furthermore, the XRD patterns of CdO:Ti-H samples show the absence of peaks arising from any Ti related phases, which confirmed the inclusion of Ti ions into the CdO lattice, without formation of separate Ti phases within CdO sample. However, since the ionic radii difference is $\sim$ 37%, following Hume-Rothery rule,[22] the substitution of Cd^{2+} ions (of radius 0.095 nm[9]) by Ti^{4+} (0.06 nm) ions forming SSS would induce distortion in the crystalline structure of host CdO. Therefore, it is expected that SSS would be formed for a very small concentrations of dopant Ti^{4+}. However with the increasing of concentration, some of the Ti-dopant ions (of oxidation state less that +4) would occupy interstital positions and accumulated on crystallite and grain boundaries (CB and GB). Theortically, it have been shown by the Authors of Ref. 23 that the formation of SSS by substitution of Cd^{2+} ions by Ti^{4+} ions would blue shift the optical bandgap (E_g). That blue shift was caused by increasing the carrier concentration, which was experimentally observed for small doping level.[16]

The sammerized results of the structural analyses of Fig. 1a are presented in Table I. The Rietveld refinement method was used to calculate the lattice parameter (a). The calculated R-parameters (R_{wp} is the weighted profile factor and S is the goodness-of-fit) indicate acceptable fitting for a single phase since the value of S parameter is in-between 1 and 2 (close to 1),[24] which can be noticed graphically in Fig. 1b. As an example, Fig. 1b shows graphically the Rietveld refinements result of the as-synthesized S4-H sample. The blue solid line (up) is the experimental data and the red solid line (up) is the calculated pattern. The pink solid line (down) is the intensity difference between the experimental and calculated-theoretical patterns, which was weak referring mainly to the formation of a single phase polycrystalline powder.

The volume of the unit cell (V_{cell}) of pristine CdO film was 101.5 Å^3, however, with hydrogenation, V_{cell} became 103.45 Å^3. The increase in V_{cell} by $\sim$ 1.9% due to the hydrogenation was attributed to

Table I. Structure analysis: Mean crystallite size (CS), crystal strain (ε), lattice parameter (a), unit-cell volume (V_{cell}) and Rietveld refining factors of the as-synthesised and hydrogenated samples

					Refinement parameters	
Sample	**CS (nm)**	**Strain ε (%)**	**a (Å)**	**V_{Cell} (Å^3)**	**R_{wp} (%)**	**S**
CdO-H	41.0	0.26	4.6987	103.73	19.78	1.38
S1-H	40.8	0.23	4.6938	103.42	12.08	1.07
S2-H	40.8	0.18	4.6933	103.39	10.19	1.55
S3-H	38.6	0.11	4.6908	103.22	14.54	1.77
S4-H	36.1	0.16	4.6918	103.29	13.49	1.38
S5-H	36.3	0.17	4.6927	103.35	11.64	1.67

Table II. Conduction parameters [resistivity (ρ), carrier (electron) mobility (μ) and carrier concentration (N_{el})], mean-free-path (mfp) and optical (measured) band gap

Sample	ρ ($\times 10^{-4}\Omega$ cm)	μ (cm^2/V s)	N_{el} ($\times 10^{20}$ cm^{-3})	mfp (nm)	E_g (eV)
CdO	201	7.03	0.44	0.51	2.27
S0-H	69.1	8.5	1.05	0.81	2.28
S1-H	15.5	22.2	1.8	2.55	2.4
S2-H	3.72	38.36	4.37	5.92	2.36
S3-H	3.47	28.7	6.9	5.16	2.06
S4-H	9.3	12.9	5.2	2.11	1.94
S5-H	17.3	16	2.26	1.98	1.64

the creation of oxygen vacancies (V_Os); similar results were observed in many previous results.[25–27]

Some of cadmium ions in sample S1-H were substituted (doped) by Ti^{4+} ions. This doping should reduce the V_{cell} due to the small size of Ti^{4+}, as shown in the inset of Fig. 1a. The inset of Fig. 1a shows decreasing in V_{cell} with increasing of Ti% doping level down to a minimum value at $\sim$ 0.6%Ti before slight increase, which attributed to the incorporation of the additional Ti ions into the interstitial locations of host CdO lattice and accumulation on GB and CB. Such Ti incorporation should be accompanied by creation of V_Os. Therefore, the V_{cell} varies by the competition of the incorporation of Ti-ions and creation of O-vacancies (V_Os). It should be mentioned that both types of incorporations have great effects on the conduction properties.

The average crystallite size (CS) and the structural strain, given in Table I, were calculated for each sample by using graphical Williamson–Hall (W–H) method. The W–H equation is,[28]

$$(\beta_{hkl}/\tan\theta_{hkl})^2 = (k\lambda/D)(\beta_{hkl}/\tan\theta_{hkl}\sin\theta_{hkl}) + 16\varepsilon^2 \quad (1)$$

where θ_{hkl} is the Bragg angle, $k \sim 4/3$, D is the crystallite size (CS), β_{hkl} is the peak width at half-maximum, ε is the strain, and λ is the used x-ray wavelength. The plot of Fig. 1c of $Y = (\beta_{hkl}/\tan\theta_{hkl})^2$ versus $X = \beta_{hkl}/\tan\theta_{hkl}\sin\theta_{hkl}$ give a straight line, from which D and ε can be determined, as shown in Fig. 1c, for S4-H sample, for example. The nano-CS given in Table I were found to be around 40 nm, and decreased from increasing Ti% doping level, which might be explained by the accumulation of additional amorphous Ti dopant ions on GB/CB due to the limited solid solubility of Ti ions in CdO lattice.

The strain values decreased from increasing Ti% doping level to its minimum value (Table I) at 0.6%Ti incorporation level and then increased. It will be seen in the next paragraph (Fig. 5) that the CPs (conductivity/resistivity, carrier mobility, and carrier concentration) get the highest values for Ti dopant level of 0.3–0.6% Ti. It means that the structural strain has also effect on the CPs in addition to other factors. In the present work, the whole results refer that $\sim$ 0.6 wt.% is the solid solution saturation limit of Ti in CdO, under that limit Ti^{4+} ions form SSS in host CdO, but with more addition of Ti ions will occupy interstitial positions in addition to CB and GB. Figure 1d shows the SEM micrographs of S4-H sample. The film has woolly-shaped elements, as that for undoped CdO[29] and the GS was estimated to $\sim$ 200 nm.

OPTICAL PROPERTIES

The corrected spectral transmittance, $T(\lambda)$ and reflectance, $R(\lambda)$ of CdO-H and CdO:Ti-H films are shown in Fig. 2. It shows, clearly that the studied films are translucent in the visible region tending to be more transparent in the NIR spectral region. The corrected spectral reflectance, $R(\lambda)$ is small and nearly constant of less than 5%. The spectral absorption coefficient $\alpha(\lambda)$ of a film of thickness d is given by $\alpha(\lambda) = \ln[(1 - R(\lambda))/T(\lambda)]/d$. The spectral $\alpha(\lambda)$ of the investigated films rapidly decreased with increasing λ, as shown in Fig. 3 due to the direct property of bandgaps. Moreover, the absorption coefficient α at 1000 nm increased from increasing Ti content level, as shown in the inset of Fig. 3. The optical band gap (E_g) can be evaluated by using Tauc technique[30]:

$$\alpha h\upsilon = A_{op}(h\upsilon - E_g)^m \quad (2)$$

where the value of m is equal to 0.5 for direct transitions, A_{op} is the constant of each film sample and $h\upsilon$ is the photon energy. Figure 4 shows $(\alpha h\upsilon)^2$ versus $h\upsilon$ plot; in which the extrapolation of the straight-line portion was used to estimate the value of the corresponding optical band gap (Table I) within an approximated accuracy of 0.05 eV. It was found that the obtained bandgap of undoped CdO-H was within the well-known standard range of values (2.2–2.6 eV).[3] With increasing Ti incorporation level, the bandgap of the host CdO:Ti-H films blue-shifted (band-gap widening—BGW) followed by red-shifting (band gap narrowing—BGN), as shown in the inset of Fig. 4. The blue-shift was observed in Ref. 15. The blue-shift (BGW) of the

absorption edge of CdO:Ti-H thin films was caused with the increase in the carrier concentration (N_{carr}), according to Moss-Burstein TCO effect.[31] While the red-shift (BGN) was also observed previously in Al-doped CdO films[32,33] and Co-doped CdO films.[34] Generally, two types of mechanisms are dominant in affecting the optical energy gap of TCO: (1) BGW and (2) BGN. It was known that the BGN starts influence by increasing the carrier concentration to 10^{18}–10^{19} cm^{-3};[35,36] Identical phenomenon was observed in ZnO:In system for carrier concentration 8.71×10^{19} cm^{-3}.[37] The large carrier concentration was observed in the present work for Ti doping level more than 0.3 wt.%, under which Ti^{4+} ions substitute the Cd^{2+} ions in host CdO lattice that will result in extra weakly bound electrons. Once the impurity band resulting from these weakly bound electrons becomes broad enough to reach the edge of the conducting band and resulted in BGN.[38–40] Therefore, the optical bandgap of CdO as TCO material is normally controlled by two contrary factors, the structural band gap (E_g^{dir}) and the Moss-Burstein (M-B) shift (E_g^{MB}): $E_g^{opt} = E_g^{dir} + E_g^{MB}$.[41] The first part, E_g^{dir} is controlled by electron-lattice interaction, which is sensitive to any microstructural alterations, like doping/incorporation effects, which generate impurity band tail broadening that merges with the conduction band causing BGN. The energy part E_g^{MB} could be affected by the variation in the carrier (electron) concentration. So, it is clear that the BGN in the measured optical bandgap E_g^{opt} was mainly due to the decrease in E_g^{dir}. The inset of Fig. 4 and Table I show that the BGN control the variation of optical E_g^{opt} defeating BGW except sample S1-H and S2-H. Table I presents steady BGN with increasing Ti% in the limit of present doping. This can be attributed to the steady increase in the density of created O-vacancies with increasing Ti% inclusion due to the strong power of Ti^{4+} ions in creation of O-vacancies under hydrogenation.[10]

In summary, the presence of dopant Ti^{4+} dopant ions have the efficient ability for dissociation of H_2 molecules into H atoms/ions that could create more O-vacancies, which is responsible for variation in band gap as well as concentration of conduction electrons.

ELECTRICAL PROPERTIES

Table II presented the values of eelectrical resistivity (ρ), carrier concentration (N_{el}) and carrier mobility (μ) for CdO-H (S0-H) and Cd:Ti-H film samples. Figure 5 demonstrated the variation of ρ, N_{el}, and μ with Ti% doping level. It shows that CPs attained their highest values in the range 0.3–0.6 Ti wt.% i.e. in the solid solution saturation limit. Figure 6 shows a similar behavior for $TC_{[111]}$ and carrier mobility (μ_{el}) versus doping level. As mentioned earlier, the reduction in carrier concentration for doping level more that 0.6%, could be attributed to the gradual accumulation of dopant Ti ions on CBs and GBs. Such accumulation creates potential barriers that effectively reduce the measured concentration of carriers and conductivity, and scatter conduction electrons during conduction process and thus reduces their mobility. Thus, the electrical results are in agreement with the structural results and responsive to the microstructural defects like grain boundaries.

The variation of the conduction parameters could be also studied through a carrier mean-free-path (mfp), which is given by: $\text{mfp} = (h/2e)(3N_{el}/\pi)^{1/3}\mu_{el}$, where μ_{el} is the electronic mobility, e is the electronic charge and h is the Planck constant.[42] The dependence of structural parameters on the variation in the mfp among the samples was plotted in Fig. 6. Similar variation trends can be clearly observed of mfp, TC, and μ_{el} versus doping level. Figure 6 shows the variation of structural parameters (Rietveld strain ε and $TC_{[111]}$) and conduction variables (μ and mfp) versus Ti%. It is clearly demonstrating the control of electrical parameters by structural parameters. The responses were the highest in the range 0.3–0.6% doping level. The present results are comparable with previous metal-doped CdO, for CdO:W[7] system of almost similar radii. Nevertheless, the CdO:Ti system is not superior from TCO point of view as other dopants like CdO:Be or CdO:Ge[43,44] prepared with identical methods and circumstances.

CONCLUSIONS

Using the evaporation method, CdO thin films incorporated different amounts of Ti ions were deposited on glass substrates. In this work, the results of the structural study, clearly demonstrate the possibility of preparing CdO films totally doped with Ti^{4+} ions with concentration up to $\sim$ 0.6 wt.%. It was found that at this concentration, the dopant Ti ions have strong influences on the structural, optical and electrical properties of host CdO films. The results, also revealed that Ti doping strongly enhanced the [111] preferred orientation growth of CdO films especially with 0.3 wt.%.

In summary, the explanations of the results are based on the fact that as Ti ions are doped in CdO, initially substitutional solid solution SSS is formed. As the Ti doping is kept on increasing, they are accumulated on CB and GB. Moreover, oxygen vacancies are also created after annealing in the H2 atmosphere.

It was observed that such type of doping could improve the TCO properties of CdO films from TCO point of view. The utmost carrier mobility of $\sim$ 40 cm^2/V s was found with CdO film doped with 0.3 wt.%Ti, which is about 6 times higher than the carrier mobility in CdO without doping. The higher carrier concentration of $\sim 7\times10^{20}$ cm^{-3} was found with Ti concentration of 0.6 wt.%. In conclusion, our

results suggest the strong possibility of using, CdO film doped with Ti within the range 0.3–0.6 wt.% in the TCO applications.

REFERENCES

1. B.G. Lewis and D.C. Paine, *Mater. Res. Soc. Bull.* 25, 22 (2000).
2. M. Yan, M. Lane, C.R. Kannewarf, and R.P.H. Changa, *Appl. Phys. Lett.* 78, 2342 (2001).
3. Z. Zhao, D.L. Morel, and C.S. Ferekides, *Thin Solid Films* 413, 203 (2002).
4. R.K. Gupta, K. Ghosh, R. Patel, S.R. Mishra, and P.K. Kahol, *Curr. Appl. Phys.* 9, 673 (2009).
5. A.A. Dakhel, *Thin Solid Films* 518, 1712 (2010).
6. R.K. Gupta, F. Yakuphanoglu, and F.M. Amanullah, *Phys. E* 43, 1666 (2011).
7. A.A. Dakhel, *J. Electron. Mater.* 41, 2405 (2012).
8. Powder Diffraction File, Joint Committee for Powder Diffraction Studies (JCPDS) file No. 05-0640.
9. R.D. Shannon, *Act Crystallogr. A* 32, 751 (1976).
10. M. Pozzo and D. Alfe, *Int. J. Hydrog. Energy* 34, 1922 (2009).
11. Haixia Chen, Jijun Ding, Feng Shi, Yingfeng Li, and Wenge Guo, *J. Alloys Compd.* 534, 59 (2012).
12. A. Davoodia, M. Tajallya, O. Mirzaeea, and A. Eshaghi, *Optik* 127, 4645 (2016).
13. R.K. Gupta, K. Ghosh, S.R. Mishra, and P.K. Kahol, *Mater. Lett.* 62, 1033 (2008).
14. K. Sakthiraj and K. Balachandra Kumar, *Int. J. ChemTech Res.* 6, 2216 (2014).
15. B. Saha, R. Thapa, and K.K. Chattopadhyay, *Solid State Commun.* 145, 33 (2008).
16. C.P. Liu, Y. Foo, M. Kamruzzaman, C.Y. Ho, J.A. Zapien, W. Zhu, Y.J. Li, W. Walukiewicz, and K.M. Yu, *Phys. Rev. Appl.* 6, 064018 (2016).
17. R.K. Gupta, K. Ghosh, R. Patel, and P.K. Kahol, *Appl. Surf. Sci.* 255, 2414 (2008).
18. R.K. Gupta, K. Ghosh, R. Patel, and P.K. Kahol, *Appl. Surf. Sci.* 255, 6252 (2008).
19. C.S. Barrett and T.B. Massalski, *Structure of Metals* (Oxford: Pergamon, 1980), p. 204.
20. A.A. Dakhel and H. Hamad, *Int. J. Thin Films Sci. Technol.* 1, 25 (2012).
21. A.A. Dakhel, *Mater. Chem. Phys.* 130, 398 (2011).
22. C. Kittel, *Introduction to Solid State Physics* (New York: Wiley, 1996), p. 425.
23. Y. Sharma and P. Srivastava, *Indian J. Pure Appl. Phys.* 49, 619 (2011).
24. L.B. McCusker, R.B. Von Dreele, D.E. Cox, D. Louer, and P. Scardi, *J. Appl. Cryst.* 32, 36 (1999).
25. S. Heo, C. Oh, J. Son, and H. Myung Jang, *Sci. Rep.* 7, 4681 (2017). https://doi.org/10.1038/s41598-017-04884-2.
26. E. Enriquez, A. Chen, Z. Harrell, P. Dowden, N. Koskelo, J. Roback, M. Janoschek, C. Chen, and Q. Jia, *Sci. Rep.* 7, 46184 (2016). https://doi.org/10.1038/srep46184.
27. A. Marthinsen, C. Faber, U. Aschauer, N. Spaldin, and S. Selbach, *MRS Commun.* 6, 182 (2016).
28. A. Khorsand Zak, W.H. Abd Majid, M.E. Abrishami, and R. Yousefi, *Solid State Sci.* 13, 251 (2011).
29. A.A. Dakhel, *Bull. Mater. Sci.* 37, 1 (2014).
30. J. Tauc and F. Abelesn, eds., *Optical Properties of Solids* (New York: North Holland, 1969).
31. J.I. Pankove, *Optical Processes in Semiconductors* (NY: Dover, 1975), p. 36.
32. I.S. Yahia, G.F. Salem, M.S. Abd El-sadek, and F. Yakuphanoglu, *Superlattices Microstruct.* 64, 178 (2013).
33. R. Maity and K.K. Chattopadhyay, *Solar Energy Mater. Solar Cells* 90, 597 (2006).
34. A.M. El Sayed and A. Ibrahim, *Mater. Sci. Semicond. Process.* 26, 320 (2014).
35. J.G. Lu and S. Fujita, *Appl. Phys. Lett.* 89, 262107 (2006).
36. A.A. Dakhel, *Opt. Mater.* 31, 691 (2009).
37. K.G. Saw, N.M. Aznan, F.K. Yam, S.S. Ng, and S.Y. Pung, *PLoS ONE* 10, e0141180 (2015). https://doi.org/10.1371/journal.pone.0141180.
38. J.J. Lu, Y.M. Lu, S.I. Tasi, T.L. Hsiung, H.P. Wang, and L.Y. Jang, *Opt. Mater.* 29, 1548 (2007).
39. Y.Z. Zhang, J.G. Lu, Z.Z. Ye, H.P. He, L.P. Zhu, B.H. Zhao, and L. Wang, *Appl. Surf. Sci.* 254, 1993 (2008).
40. J.M. Langer, C. Delerue, M. Lannoo, and H. Heinrich, *Phys. Rev. B* 38, 7723 (1988).
41. Mario Burbano, D.O. Scanlon, and G.W. Watson, *J. Am. Chem. Soc.* 133, 15065 (2011).
42. M. Chen, Z.L. Pei, X. Wang, Y.H. Yu, X.H. Liu, C. Sun, and L.S. Wen, *J. Phys. D Appl. Phys.* 33, 2538 (2000).
43. A.A. Dakhel, *Mater. Res.* 18, 222 (2015).
44. A.A. Dakhel, *Solid State Sci.* 25, 33 (2013).